Effect of Column Foot Tenon on Behavior of Larch Column Base Joints Based on Concrete Plinth

Xiaoli Han,[a,b] Jian Dai,[b,c,*] Wei Qian,[b,c,*] Baolong Li,[d] Yuanjun Jin,[a,b] and Ting Jiang [a,b]

The wooden columns in timber structures of ancient buildings have column foot tenons of various sizes. The main reason for these differences is their use for different roof loads. Six full-scale specimens with different sizes of column foot tenon were designed and manufactured. The tree species used for the specimens was larch. The quasi-static test was conducted on the specimens that were used in timber structures of ancient buildings. The effects of column foot tenon size on the mechanical properties of larch wooden columns were studied. The moment-rotational angle hysteretic curves, moment-rotational angle skeleton curves, ductility, stiffness degradation, energy dissipation capacity, slippages between the wooden column and the plinth, and the damage of the column foot tenons were examined. The test results showed that the column foot tenon played an important role in the mechanical behavior of the wooden column under low-cycle reversed cyclic loading. The rotation of the column foot tenon improved the energy dissipation capacity of the wooden column. As the rotational angle of the column base increased, the column foot tenon had different degrees of damage. Different sizes of column foot tenon had their own advantages and hysteretic behavior.

Keywords: Ancient timber structures; Wooden column; Larch; Column foot tenon; Hysteretic behavior; Concrete plinth

Contact information: a: College of Architecture and Civil Engineering, Beijing University of Technology, Beijing, 100124, China; b: College of Architecture and Urban Planning, Beijing University of Technology, Beijing, 100124, China; c: Beijing Research Center of Historic Building Protection Engineering, Beijing, 100124, China; d: Beijing Beiguo Construction Engineering Co., Ltd., Beijing, 100068, China;
** Corresponding authors: hanxiaoli221@emails.bjut.edu.cn; qianwei@bjut.edu.cn*

INTRODUCTION

Ancient timber structures are an important component of Chinese culture and Chinese civilization. Ancient timber structures have been used for thousands of years (Chang *et al*. 2019), and they constitute a complete and independent structural system. The timber structures have extremely high research value, and they mostly have been built with wood in ancient Chinese buildings (Li *et al*. 2015). However, the timber structures of ancient buildings are inevitably subjected to various loading effects over time, such as earthquake actions and wind actions. Due to the long-term effect of these loads, the safety of ancient timber structures is often compromised.

The unique value status and special mechanical properties of ancient timber structures have attracted the attention and research of many scholars. A theoretical model of restoring the moment of the column foot joint was proposed, and the proposed model was verified with a finite element model (He and Wang 2018). A quasi-static test was used to study the appropriateness of the judging conditions for the uplifting of the plinth of ancient timber structures (He *et al*. 2017a). In addition, it was used to study the effect of

high-diameter ratios (He *et al*. 2018) and different vertical loads (He *et al*. 2017b) on the mechanical properties of wooden columns. The non-linear finite element model of the column base joint (Wang *et al*. 2018) based on the rocking mechanism of the wooden column and the stress state of the column base was verified by a full-scale model with a pseudo-static test. The rocking characteristics of the first-class frame of ancient building timber structures under horizontal conditions were studied *via* a combination of theoretical derivation and finite element simulation (Wan *et al*. 2020). The shaking table test and the pseudo-static test were used to study the sliding motion between the wooden columns and the foundation stone and analyze the equilibrium relationship of the bending moment action of wooden column and restoring force characteristics caused by the column rocking of Japanese traditional wooden frames (Maeno *et al*. 2007). The quasi-static test was adopted for the traditional houses in southern Sichuan to study the lateral resistance provided by the masonry infilled Chuandou timber frames (Qu *et al*. 2020). A theoretical model of the rotational performance of the gapped Nuki joint that considered Hook's law and Hankinson's formula was established to predict the rotational stiffness and the initial slip of the Nuki joints (Shao *et al*. 2006). Shaking table and quasi-static tests were conducted on the wooden frame of Japanese ancient buildings without walls, and the horizontal restoring force was mainly determined by the bending moment resistance from tie beams and the restoring force due to column rocking (Suzuki and Maeno 2006). Local compression tests on a specified angle (Lee *et al*. 2009) on a wooden column in ancient Japanese buildings were conducted to study the skeleton curve of moment-rotation relation of the wooden column base. The results of the shaking table and static lateral load tests on the traditional wooden frame in Japan showed that the restoring force characteristics caused by the column swing and the bending moment of the tie-beam play an important role in traditional wooden structures (Kusunoki *et al*. 2003). Full-scale vibration tests and numerical analysis were used to study the sliding behavior of columns directly placed on flat stone foundations in Japanese traditional wooden buildings (Mukaibo *et al*. 2008).

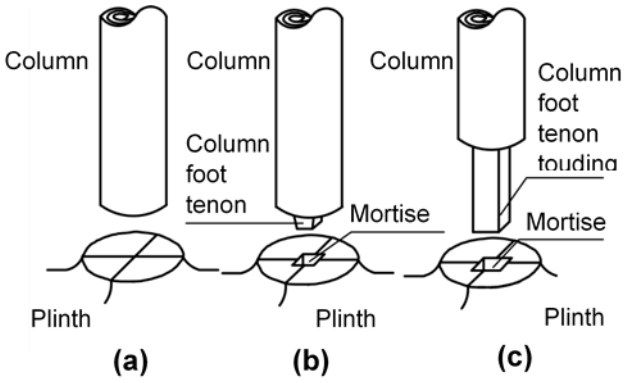

Fig. 1. Types of wooden columns on the plinth

In previous studies, the wooden columns were placed directly on the pillar foundation. However, after reviewing the literature on the timber structure of ancient buildings and on-site investigation of the wood columns in ancient buildings, it was found that the wooden columns are not all placed in this way. The description of the column foot tenon is recorded in the relevant ancient architectural literature (Yunli 1734; Bai and Wang 2000; Ma 2003). There are three ways to place wooden columns on the foundation

according to the ancient architectural documents (Ma 2003): (1) placed directly on the plinth (Fig. 1a); (2) placed on the column foot tenon (Fig. 1b); (3) placed on the touding tenon ("touding" is the name for a type of the column foot tenon in ancient timber structures.) (Fig. 1c).

Fig. 2. Plinth of Qing Dongling (Zunhua, Hebei, China)

Yunli (1734) described the wooden column foot tenon as follows: "each column is one foot in diameter, plus three inches of upper and lower tenons". During the migration of Yongle Palace in the Yuan Dynasty (Bai and Wang 2000), it was found that there were tenons at the foot of the inner columns that existed in the Shanxi Province of China (The Institute for History of Natural Sciences 1985).

Secondly, the use of column foot tenons can be observed in the column foundation ruins of the ancient buildings on the site. Figures 3 through 8 illustrate the remnants of the plinth at the cultural relics site.

Fig. 3. Plinth ruins in the renovation of Nanjing Drum Tower (Nanjing, Jiangsu, China).

Fig. 4. Plinth ruins of Qing Dongling (Zunhua, Hebei, China)

Fig. 5. Plinth of Sima Jinlong tomb in Northern Wei Dynasty (Datong, Shanxi, China)

Fig. 6. Plinth of Shentong Temple in Sui Dynasty (Jinan, Shandong, China)

Fig. 7. Ruins of Panlong Plinth in the central capital of Ming Dynasty (Fengyang, Anhui, China)

Fig. 8. Plinth of Shentong Temple in Sui Dynasty (Jinan, Shandong, China)

In this study, six full-scale specimens with different sizes of column foot tenon were subjected to quasi-static loading to investigate the mechanical properties of the column base joints with column foot tenons. The tree species used for the specimens was larch. The details of the specimens, the experimental program, and the experimental results and analysis are reported in the following sections.

EXPERIMENTAL

Specimen Design

According to Figs. 1 through 8 and other preliminary works (Ma 2003; Ssu-Ch'eng 2006; BMCC 2007), six full-scale specimens with different sizes of column foot tenon were designed and manufactured. The details of six full-scale specimens are shown in Table 1. The different sizes of column foot tenons and plinth models are shown in Fig. 9. All specimens had a height of 2310 mm. The six specimens had a circular section of 210 mm in diameter. The height:diameter ratio of the specimens was 11:1. The depth of wooden column foot tenon was equal to the diameter of the column foot tenon, and the depth of CC-6 wooden column foot tenon was 3/10D.

Table 1. Test Data of Six Specimens

ID	Size of Wooden Column Foot Tenon	Material
CC-1	*d*/*D* = 0	Larch
CC-2	*d*/*D* = 1/10	
CC-3	*d*/*D* = 1/4	
CC-4	*d*/*D* = 3/10	
CC-5	*d*/*D* = 6/10	
CC-6	*d*/*D* = 1/1	
*Note: *d* is the diameter of the wooden column foot tenon and *D* is the diameter of the wooden column.		

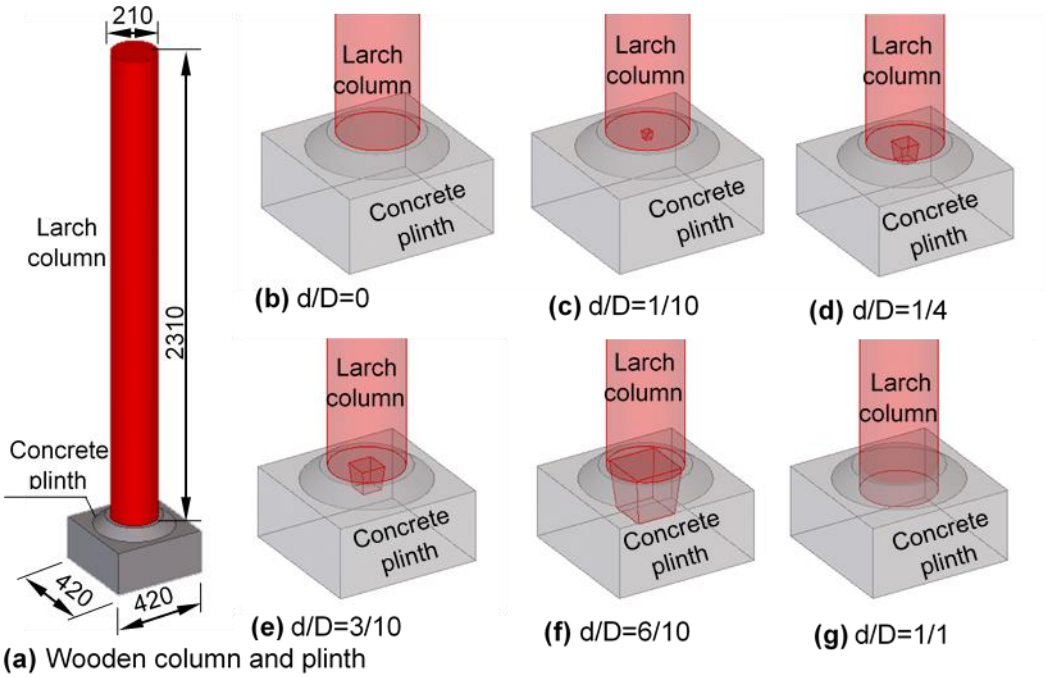

Fig. 9. Model of wooden column and plinth and column base joints

The use of the plinth in the Qing Dynasty is shown in Fig. 10. Plinth material was concrete.

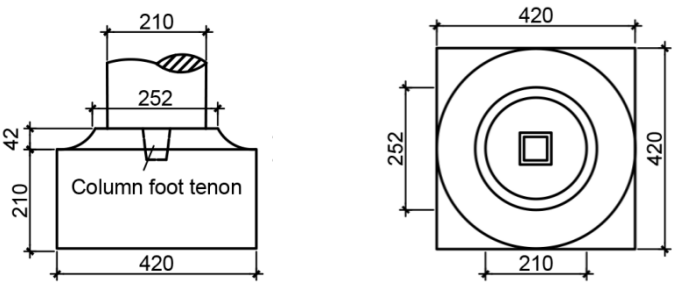

(a) Front elevation **(b)** Floor plan

Fig. 10. Use of the Plinth in Qing Dynasty

Material Properties

Larch was used as the wood for all specimens in this experiment, as it is representative of the tree species commonly used in ancient timber structures. The material properties of the specimens were tested according to GB/T 1938 (2009), GB/T 1936.1 (2009), GB/T 1935 (2009), and other relevant regulations. The data obtained from the material property tests are shown in Table 2, and results referred to defect-free small-scale specimens. The specimens are based on a water content of approximately 12% according to GB/T 1928 (2009).

Table 2. Test Values of Material Properties of Specimen

Tensile Strength Along Grain (MPa)	Compressive Strength Along Grain (MPa)	Shear Strength Along Grain (MPa)	Bending Elastic Modulus (MPa)	Bending Strength (MPa)
132.58	49.60	10.82	14060	100.35

Methods

The experiment was conducted at the Engineering Structure Experiment Center of the Beijing University of Technology (Beijing, China).

A vertical constant load was applied to the wooden column head by a 150 kN horizontally free-sliding jack along the axis of the wooden column. The lateral jack was connected to the wooden columns through specially designed jigs to facilitate lateral load transfer to the columns. The loading device is shown in Fig. 11. The direction of the loading device model in Fig. 11 was referred to Fig. 13, and the horizontal actuator was in the east of the column.

The locations of the transducers are shown in Fig. 12, and the test loading site is shown in Fig. 13. The six vertical transducers (V_1 to V_6) were mounted to the side of the wooden column to measure the vertical displacement of the column. The lateral displacement of the column was obtained by seven horizontal transducers (H_1 to H_7). The lateral displacement of the column head was measured by the horizontal sensor H_8. The original position of the column base was marked with blue before the test to observe whether the column base slipped during the test. If the column base slipped, the sliding position was marked with red.

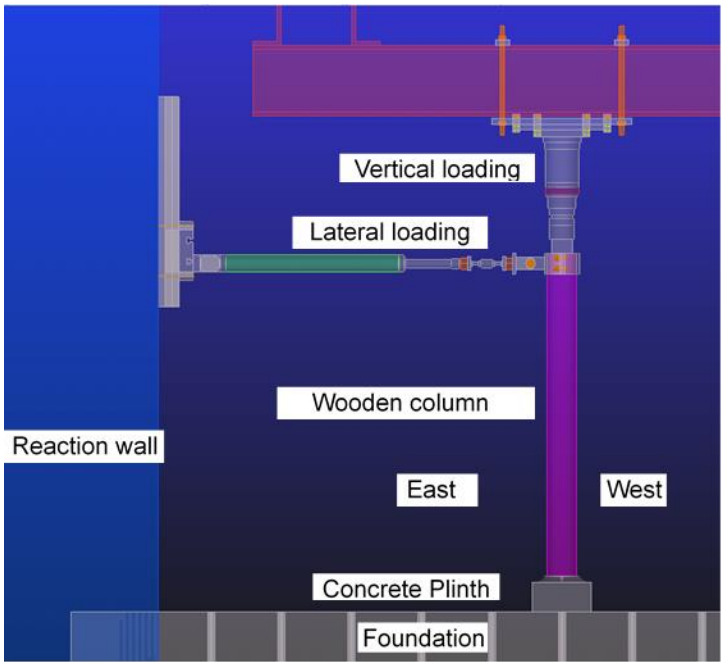

Fig. 11. Loading device

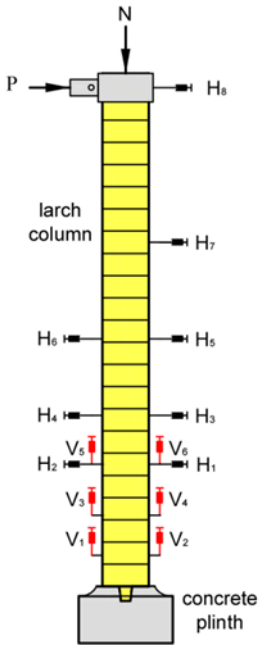

Fig. 12. Locations of the transducers

Fig. 13. Test loading site

According to ISO16670 (2003) and JGJ/T 101 (2015), cyclic loading was performed with increasing amplitudes of displacement (Fig. 14), and three cycles of loading were performed for each amplitude. When the control displacement was below 30 mm, the increment amplitude was 5 mm. Above 30 mm displacement, the increment amplitude was 10 mm.

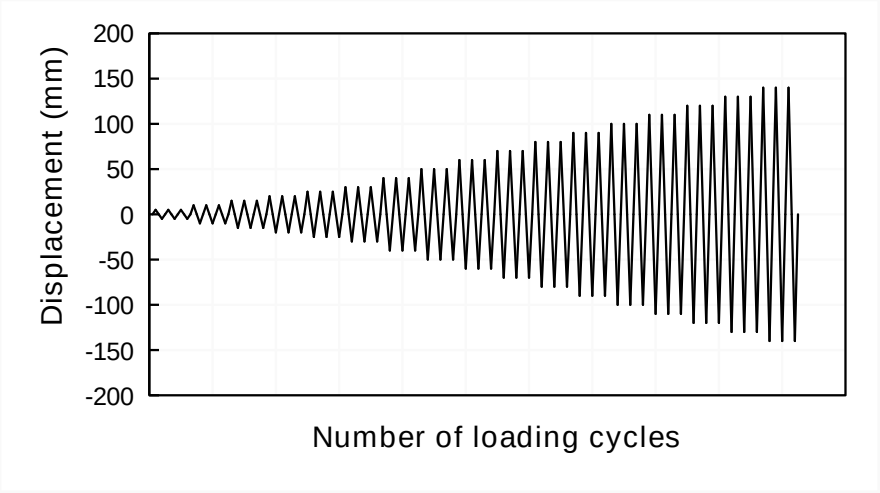

Fig. 14. Loading protocol

RESULTS AND DISCUSSION

Test Phenomenon

The main experimental phenomena of the columns were as follows:

(1) As the loading of the specimen changed from small to large, the test phenomenon became more obvious. As the rocking of the specimen and the uplifting of the column foot became obvious, the contact part of the column foot and the plinth gradually produced an audible sound, and the interaction between the wooden column and the plinth gradually increased. The column foot was pushed uplifting (Fig. 15a), and the column foot was pulled uplifting (Fig. 15b).

(2) Specimen CC-1 slipped during loading (Fig. 15c). When the column foot tenon of CC-2 was damaged (Fig. 16a), the movement of the specimen was no longer restricted, and slippage began (Fig. 15d).

(3) There were squeezing marks at the maximum displacement in the positive and negative directions of the column foot. The column foot tenon was particularly squeezed. Figure 16b illustrates that the CC-3 column foot tenon was squeezed, and Fig. 16c shows that the CC-4 column foot tenon was worn. Figure 16d shows that the CC-5 column foot tenon was worn. Figure 16f shows the wear and tear and squeezing marks of the CC-6 column foot tenon. The compression deformation of the column foot of the wooden column and the wear and tear of the column foot tenon mainly appeared at the maximum displacement in the positive and negative directions of the specimen.

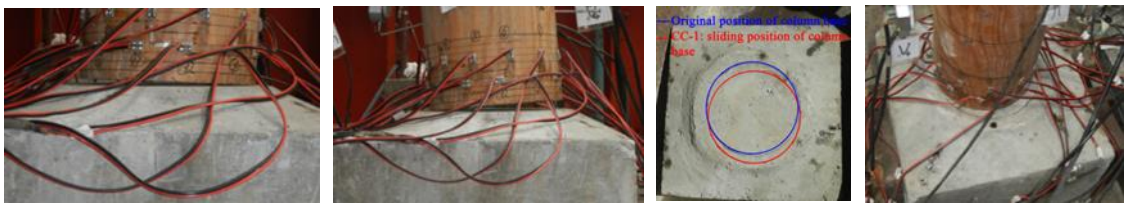

(a) uplifting pushing **(b)** uplifting pulling **(c)** CC-1 Slippage **(d)** CC-2 Slippage

Fig. 15. Uplifting and slippage

(a) CC-2 **(b)** CC-3 **(c)** CC-4 **(d)** CC-5 **(f)** CC-6

Fig. 16. Damage of column foot tenons

Stress Analysis of Column Base

Figures 17 shows that the wooden column was in the instantaneous equilibrium state when the wooden column was pulled and pushed to maximum displacement. The forces generated by the column base when the column was loaded included reaction force (R), friction force (F), and moment (M_{bc}). The moment of the column base was obtained with Eq. 1,

$$M_{bc} = N\Delta + Ph \quad (1)$$

where N is the vertical load (kN) on the column head, P is the lateral force (kN) on the column head, Δ is the lateral displacement (mm), and h is the height (mm) of the wooden column specimen. The rotational angle (θ) of the column base in the horizontal push-pull direction was calculated with Eq. 2:

$$\theta = \text{Arctan}\,(\Delta / h) \approx \Delta / h \quad (2)$$

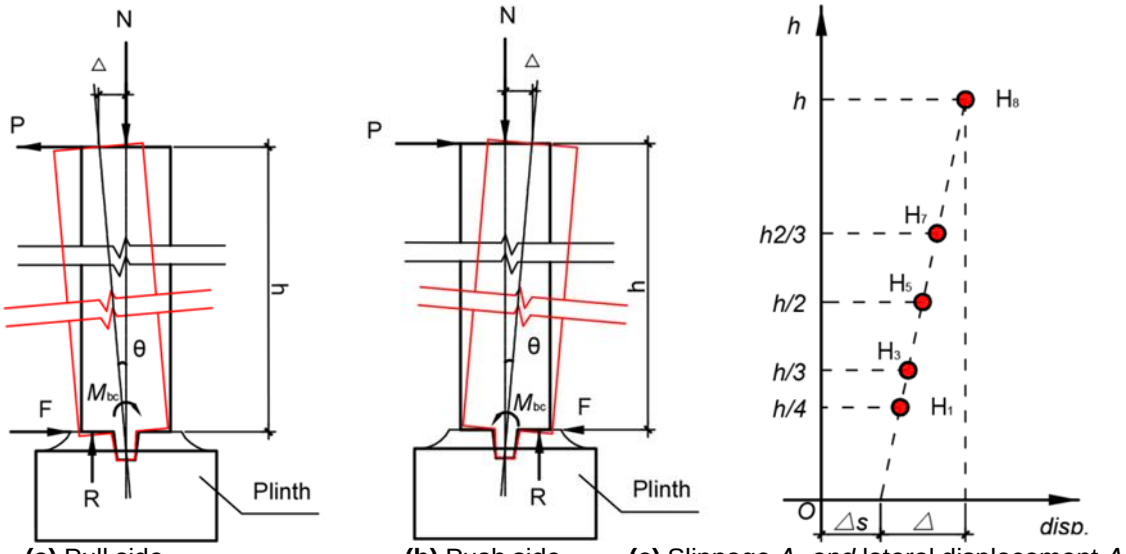

(a) Pull side **(b)** Push side **(c)** Slippage Δ_s *and* lateral displacement Δ

Fig. 17. Balance state of wooden column

Hysteretic Curves

The hysteretic curve is a curve that describes the change in the moment of the column base joint of the specimen with the rotational angle in the quasi-static test. According to the test data combined with Eq. 1 and Eq. 2, the moment-rotational angle hysteretic curve of specimens was obtained (Fig. 18).

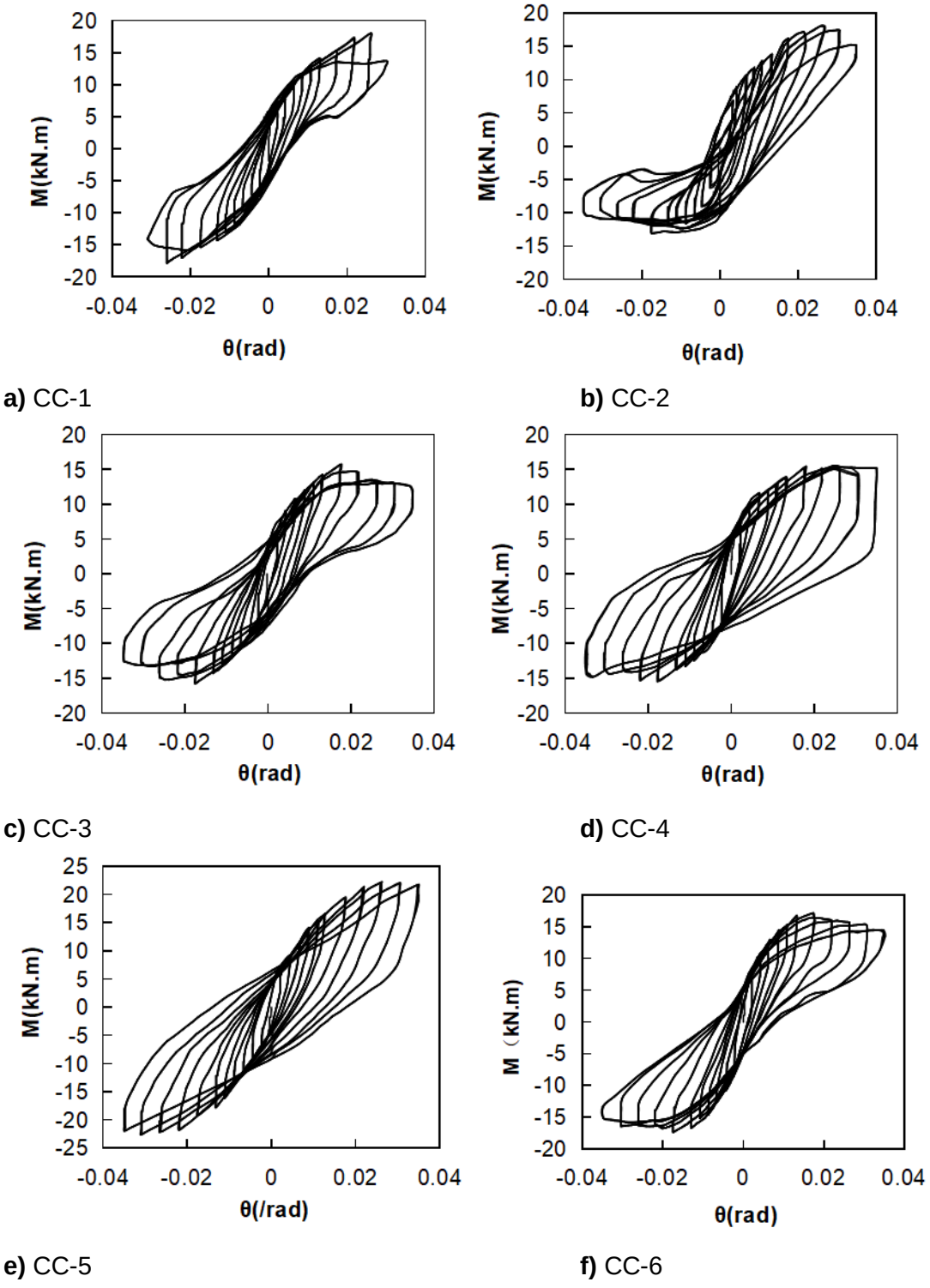

Fig. 18. Hysteretic curve of CC-1 (a), CC-2 (b), CC-3 (c), CC-4 (d), CC-5 (e), and CC-6 (f)

The hysteretic curves of the wooden columns were in the shape of an “arc,” the push and pull sides were anti-symmetric, and the hysteretic curves had a certain degree of a "pinch-up" effect. There were two reasons for this. The first reason was the initial cracks caused by the shrinkage of the specimens during curing, and the second reason was the

limiting effect of the wooden column foot tenon. At the beginning of loading, the rotational angle of the column base was small, and the deformation of the specimens was minor. When the rotational angle was small, the component was still in the elastic stage, the area of the hysteretic loop was small, and the moment of the column foot increased rapidly. As the loading displacement increased, the deformation of the wooden column gradually increased, the area of the hysteretic loop gradually increased, the curve growth began to gradually steepen, the slope gradually increased, and the resistance moment of the column foot gradually increased. When the moment reached the maximum value, the curve growth gradually slowed down, the slope gradually decreased, and the column foot resisted the bending moment. When the moment of the column foot reached the maximum value, the rotational angle of the column foot continued to increase, and the moment of the column foot gradually decreased.

The hysteretic curve of the CC-2 wooden column gradually exhibited asymmetry as rotational angle increased. The greater the rotational angle was, the more obvious the asymmetry appeared. This result occurred because the column foot tenon of the CC-2 specimen had been damaged (Fig. 16a), CC-2 split (Fig. 15d), and the sliding of the CC-2 wooden column could not be further restricted. When the moment of the CC-3, CC-4, CC-5, and CC-6 specimens reached the maximum value, the recovery of the hysteretic curve began to weaken, and the column foot tenon of the specimen began to work. The column foot of CC-6 was completely embedded in the column base, and the performance of the column foot node was closer to that of a rigid knot.

The test results showed that the hysteretic curve of the wooden column with the column foot tenon under the low-cycle reversed cyclic loading was basically arch shaped, and the forward and reverse parts were anti-symmetric. As the size of the column foot tenon increased, the influence on the hysteretic curve increased.

Skeleton Curve

The skeleton curve generally refers to the envelope of the peak point of each hysteretic curve obtained by the component of the low-cycle reversed cyclic loading test. According to the analysis results of the test data and the moment-rotational angle hysteretic curve, the moment-rotational angle skeleton curves of the specimens were obtained (Fig. 19).

Figure 19 shows that the skeleton curve of the wooden column was anti-symmetric. In the initial stage of specimen loading, the small rotational angle acting on the column foot produced a larger column foot moment, and the skeleton curve of the wooden column developed approximately linearly. As the rotational angle continued to grow, the moment increased. After the moment of the column foot reached its peak, the skeleton curve gradually became smoother as the rotational angle of the column foot continued to increase.

Table 3. Peak Value of the Moments of Wooden Columns CC-1 ~ CC-6 (kN.m)

ID	M_+	M_-	Average Value
CC-1	18.048	17.849	17.95
CC-2	18.055	11.947	15.00
CC-3	15.166	15.320	15.24
CC-4	15.380	15.118	15.25
CC-5	22.202	22.635	22.42
CC-6	16.800	17.341	17.07

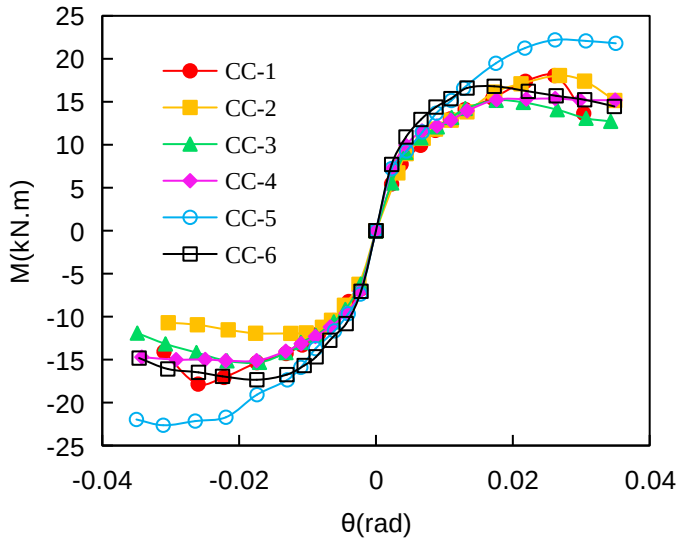

Fig. 19. Skeleton curves of specimens CC-1 to CC-6

In the early stage of loading, the column foot tenon had little effect on the skeleton curve of the wooden column. Due to the limitation of the column foot tenon, the degree of decline for each specimen was different. The peak values of the column foot moments (The peak values of the column foot moments were taken from the average value of the positive and negative peak values, Table 3) of CC-1, CC-2, CC-3, CC-4, CC-5, and CC-6 were 17.95 kN.m, 15.00 kN.m, 15.24 kN.m, 15.25 kN.m, 22.42 kN.m, and 17.07 kN.m, respectively, which represents an increasing trend. After the skeleton curve of CC-1 declined, it eased again and then continued to decline. This result occurred because the column foot tenon of the CC-1 wooden column was placed directly on the plinth. As the rotational angle of the column foot increased, the specimen slipped (Fig. 15c). The skeleton curve of the CC-2 wooden column gradually exhibited asymmetry as the rotational angle of the column foot increased. This result was due to the damage of the column foot tenon of the CC-2 wooden column. The specimen began to slip (Fig. 15d and Fig. 16a), and the column foot tenon lost its binding force on the wooden column. The skeleton curves of CC-3 and CC-4 did not differ substantially in the early stage. In the latter stage, the limiting effect of the CC-4 wooden column foot made its moment greater than that of the CC-3 wooden column. The column foot tenon of the CC-5 wooden column was a touding tenon, which was a special case. The impact of the column foot tenon on the wooden column was more obvious. After reaching the peak moment, the impact of the column foot tenon on the wooden column decreased the slowest. The peak lateral force of wooden column CC-5 was the highest, and it can be considered that this type column foot tenon of column could resist greater horizontal loads, which is why it was often used in buildings with high terrain and high wind load. Its role was to strengthen the stability of the buildings. The column foot of the CC-6 wooden column was generally used in civil buildings. The frame load of civil buildings was far less than that of official buildings, so it was necessary to restrict the movement of the column foot to provide additional safety.

The test results showed that the column foot tenon of the wooden column noticeably improved the moment of the column foot of the wooden column under low-cycle reversed cyclic loading.

Ductility

The ductility of components usually have been evaluated by the ductility factor (μ). The ductility factor was calculated as the ratio between the maximum deformation u_{max} and the yield deformation u_y (Porcu 2017). The ductility factor (μ) of the column base was calculated with Eq. 3,

$$\mu = u_{max}/u_y \quad (3)$$

where u_{max} is the maximum deformation (rad), u_y is the yield deformation (rad).

Wood is an anisotropic material, and there was no clear definition of yield. The results of using one method to obtain the yield deformation is not very accurate, so three methods were selected to obtain the yield deformation of the specimens. According to the moment-rotational angle skeleton curves and related parameters, the Geometric Graphic method (Guo *et al*. 2003), the Equivalent Elasto-Plastic Energy method (Guo *et al*. 2003, He *et al*. 2018), and the Park method (Guo *et al*. 2003), were used to obtain the yield deformation and the maximum deformation of the specimens. According to the results and Eq. 3, the ductility factors of the specimens were calculated, and the average values were taken as the characteristic parameter of the ductility factors of the wooden column. The ductility factor (μ+) of CC-5 was taken as an example, and the yield deformations and maximum deformations are shown in Fig. 20 and Table 4. The ductility factors (μ+) are shown in Table 4.

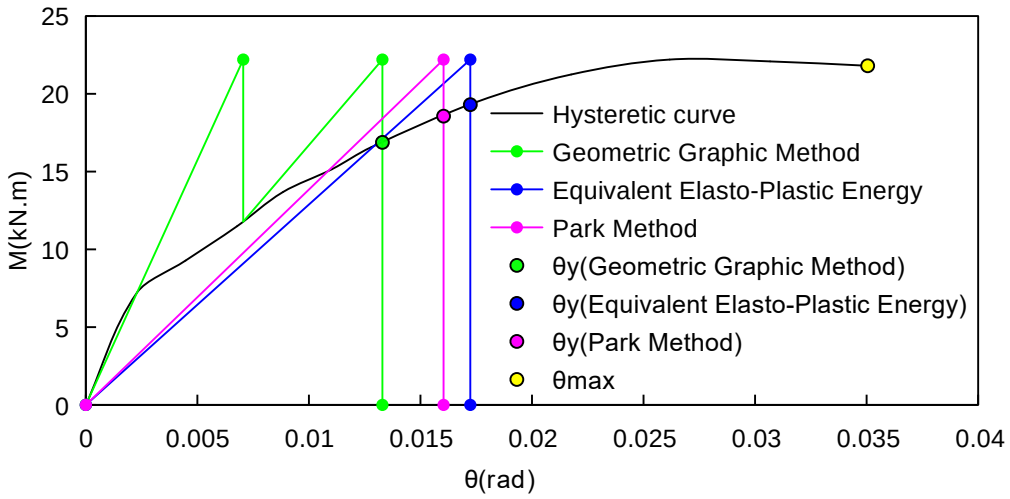

Fig. 20. Three analysis methods of CC-5 ductility factor

Table 4. Value of the Ductility Factor of Wooden Columns CC-5 (μ+)

Methods	u_y	u_{max}	(μ+)
Geometric Graphic method	0.0132	0.0350	2.64
Equivalent Elasto-Plastic Energy method	0.0160	0.0350	2.19
R. Park method	0.0172	0.0350	2.03
Average Value	-	-	2.29

The calculation and analysis results of the specimens in this test are shown in Table 5 and Fig. 21.

The pushing and pulling ductility factor of the CC-2 wooden column were different because the column foot tenon of the CC-2 wooden column was damaged, and the

specimen slipped (Fig. 15d and Fig. 16a). Table 5 and Fig. 21 show that the ductility factors of CC-1, CC-2, CC-3, CC-4, CC-5, and CC-6 were 2.15, 3.11, 3.34, 4.04, 2.31, and 4.03, respectively. The ductility factors of the 6 specimens were all greater than 1, which showed that the deformation ability of the wood column was good, the material was not easily damaged, and it had good ductility. The ductility factors of the 6 specimens indicated that the increase of CC-2, CC-3, CC-4, CC-5, and CC-6 were 44.4%, 55.2%, 88.0%, 7.4%, and 87.6%, respectively, relative to CC-1. Therefore, the column foot tenons improved the ductility of the wooden column. The CC-1 wooden column was placed directly on the plinth, and the ductility of the specimen was partly weakened. The CC-3, CC-4, CC-5, and CC-6 specimens with column foot tenons were compared again with CC-2, and the increase of CC-3 CC-4, CC-5, and CC-6 were 7.52%, 30.21%, -25.62%, and 29.89%.

Table 5. Values of the Ductility Factors of Wooden Columns CC-1 to CC-6

ID	μ+	μ -	Average Value
CC-1	1.99	2.32	2.15
CC-2	2.30	3.92	3.11
CC-3	3.36	3.32	3.34
CC-4	4.10	3.99	4.04
CC-5	2.29	2.34	2.31
CC-6	4.09	3.97	4.03

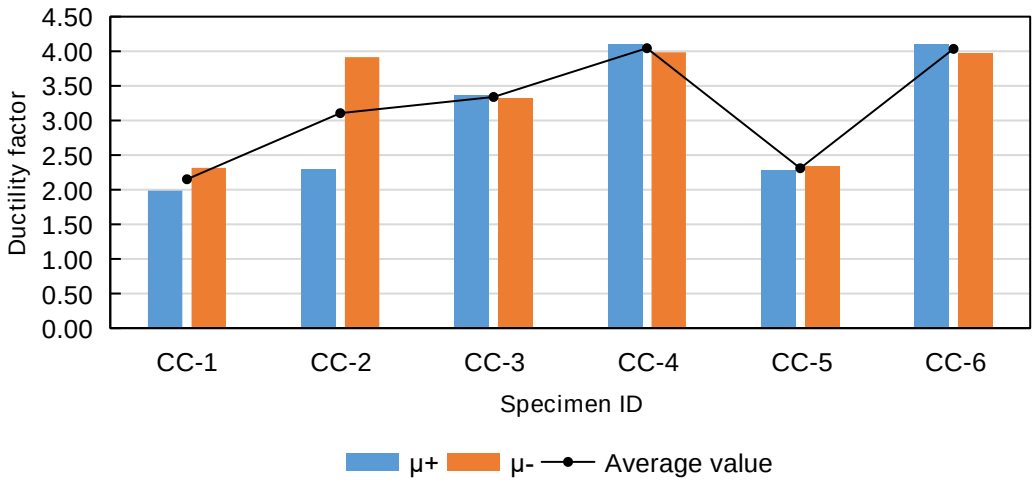

Fig. 21. Ductility factors for specimensCC-1~CC-6

Figure 21 shows that the ductility factors of the six specimens reached the maximum value for the CC-4 specimen. The ductility factor of the CC-2 wooden column was small due to damage of the column foot tenon (Fig. 16c), and the CC-2 specimen slipped (Fig. 16a). The size of the column foot tenon continued to increase, and the ductility factor of the wooden column increased accordingly. The ductility factor of CC-3 relative to CC-2 was improved by 7.5%, and the maximum increase of CC-4 was 30.2%. As the column foot tenon continued to increase, the ductility factor of the CC-5 column foot tenon decreased by 25.6%. The ductility factor of the CC-6 column foot tenon used in civil buildings increased 29.9%. The column foot tenon continued to increase, and the ductility of the wooden column was reduced.

The test results illustrated that the column foot tenon of the wood column affected the ductility of the wood column under the low-cycle reversed cyclic loading. However, increases in the size of the column foot tenon were not uniformly related to improved ductility.

Stiffness Degradation

During the loading process of the test, the rotation stiffness of the wooden column gradually decreased as the number of cycles and the rotational angle increased, which caused the stiffness of the component to deteriorate. The stiffness degradation of the wooden column can be expressed by the rotation stiffness (K_i) of the specimen.

The expression of the rotation stiffness (K_i) corresponding to the rotational angle at each level was expressed with Eq. 4,

$$K_i = (|+M_i|+|-M_i|) / (|+\theta_i|+|-\theta_i|) \quad (4)$$

where K_i is the rotation stiffness of the specimen under the i-th control rotational angle, θ_i is the rotational angle of the specimen under the i-th control displacement, and Mi is the column foot moment of the specimen under the i-th control rotational angle.

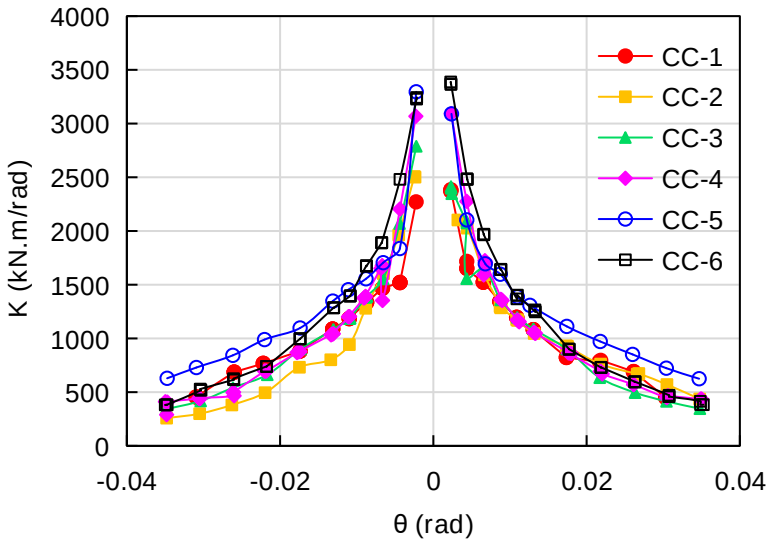

Fig. 22. Stiffness degradation curves of specimens CC-1 to CC-6

According to the test data analysis and the moment-rotational angle hysteretic curves, the stiffness degradation curves of specimens were obtained with Eq. 4 (Fig. 22). Figure 22 shows that the stiffness degradation trends of the six specimens were generally similar, and the details were slightly different, which was due to the sizes of the column foot tenons. The stiffness of the wood column deteriorated faster in the early stage and then slowed down in the later stage. In the early stage of loading, the rotational angle of the column foot was small. Then, none of the specimens were damaged, so the stiffness of the wooden column was large. As the rotational angle increased, the specimen gradually broke down, and the stiffness of the wooden column deteriorated noticeably. When the rotational angle increased, the column foot tenon of the wood column started to play a role, and the stiffness degradation phenomenon was subtle. Then, the rotational angle increased, the damage of the specimen increased continuously, and the stiffness continued to deteriorate. Comparing the stiffness degradation curves of the 6 wooden columns, the relationships

between the initial stiffnesses and the sizes of the column foot tenons were: CC-6 > CC-5 > CC-4 > CC-3 > CC-2 > CC-1. In addition, the initial stiffness increased as the size of the column foot tenon increased. When the rotational angles were loaded to the maximum, all of the rotation stiffnesses were greater than 0, and the members still had the ability to rotate.

The test results showed that the column foot tenon of the wood column had a noticeable limiting effect on the stiffness degradation of the wood column under low-cycle reversed cyclic loading.

Energy Dissipation Capacity

The energy dissipation capacity of the wooden column is measured by the area enclosed by the hysteretic curve of the specimen. It is usually evaluated by the equivalent viscous damping ratio (ζ_{eq}). This is shown in Eq. 5,

$$\zeta_{eq} = E_{DS} / (2\pi E_S) \quad (5)$$

where E_{DS} is the area of the hysteresis loop (m^2), which is represented by $E_{DS} = S_{(ABC + CDA)}$, $S_{(ABC + CDA)}$ is the area enclosed by the hysteresis curve in Fig. 23, E_S is the elastic potential energy (m^2), and $E_S = S_{(OBE + ODF)}$, $S_{(OBE + ODF)}$ is the sum of the areas of triangle OBE and ODF in Fig. 23.

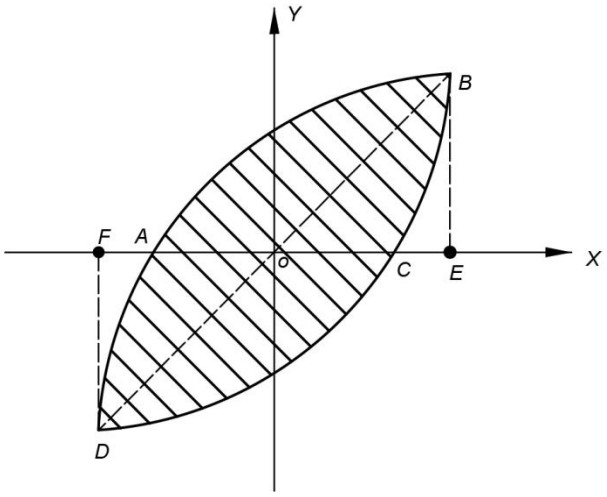

Fig. 23. Calculation of the equivalent viscous damping ratio

Figure 24 shows the equivalent viscous damping ratio curves of specimens CC-1, CC-2, CC-3, CC-4, CC-5, and CC-6. Figure 24 shows that the equivalent viscous damping ratio trends of the six wooden columns were approximately the same, and the details were slightly different because of the size of the column foot tenons.

As the rotational angle of the CC-1 specimen increased, the equivalent viscous damping ratio curve decreased more obviously. When the member began to slip (Fig. 15c), the trend of the equivalent viscous damping ratio curve slowed down. The sliding of the components had a certain limiting effect on the equivalent viscous damping ratio of the wooden column. When the rotational angle of the CC-2 specimen was small due to the limitation of the column foot tenon, the downward trend of the equivalent viscous damping ratio curve was slower than that of specimen CC-1. The column foot tenon was broken (Fig. 16a), the specimen began to slip (Fig. 15d), and the development trend of the equivalent viscous damping ratio curve of the CC-2 specimen was similar to that of

specimen CC-1. The initial equivalent viscous damping ratio of specimen CC-4 was greater than that of specimen CC-3, and the influence of the column foot tenon of the specimen CC-3 on the equivalent viscous damping ratio was noticeably higher than that of specimen CC-4. Due to the large size of the column foot tenon of specimen CC-5, the rotation of the specimen was restricted, and the effect on the energy dissipation capacity was weaker than that of specimen CC-4. When the rotational angle was small, the effect of specimen CC-6 on the equivalent viscous damping ratio was stronger than that of the CC-5 wood column, and when the rotational angle increased, the effect on the equivalent viscous damping ratio was weaker than that of column CC-5. Then the behavior of the CC-6 column base joint was stronger than CC-5 at the early stage, but was weaker at the last stage.

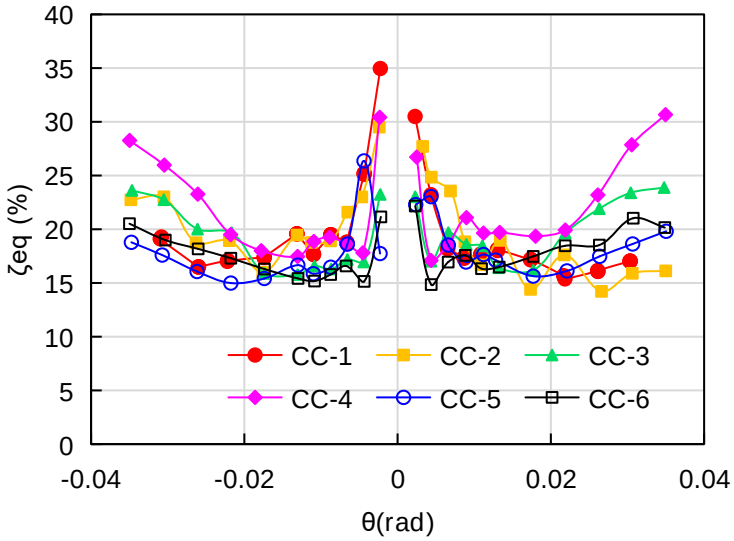

Fig. 24. Equivalent viscous damping ratio curves of specimens CC-1 to CC-6

The test results showed that the column foot tenon of the wooden column had a noticeable effect on improving the energy dissipation capacity of the wooden column under low-cycle reversed cyclic loading.

CONCLUSIONS

1. The shape of the hysteretic curves exhibited a certain degree of "pinch-up" effect. The initial cracks caused by the shrinkage of the wooden column during curing and the limiting effect of the wooden column foot tenon were responsible for this.
2. The failure of the column foot tenons of the wooden columns occurred through damage, slippage, and rotation.
3. The ductility factor of all specimens exceeded 2. The column foot tenons of the wood columns had an obvious effect on the ductility of the wood columns under the low-cycle reversed cyclic loading. However, increases in the size of the column foot tenon were not uniformly related to improved ductility. The ductility of the wooden column was affected by the damage of the column foot tenon.

4. The relationships between the initial stiffnesses and the sizes of the column foot tenons were: 1-1D > 6/10D > 3/10D > 1/4D > 1/10D > 0D. As the size of the wooden column foot tenons increased, the rigidity of the components increased.
5. The relationships between the initial equivalent viscous damping ratios of the wooden columns and the sizes of the column foot tenons were 0D > 3/10D > 1/10D > 6/10D > 1/4D > 1-1D. The slippage of the column base and the rotation of the column foot tenon dissipated part of the energy under low-cycle reversed cyclic loading.

ACKNOWLEDGMENTS

The authors thank the National Natural Science Foundation of China (Grant No. 51678005) for their support.

REFERENCES CITED

Bai, L.-J., and Wang J.-F. (2000). *Official Building Structure in the Qing Dynasty*, Beijing University of Technology Press, Beijing, China.

Beijing Municipal Commission of Construction (BMCC) (2007). *Chinese Ancient Building Construction Technology*, China Architecture & Building Press, Beijing, China.

Chang, L.-H., Chang, X.-H., Chang, H., Qian, W., Cheng, L.-T., and Han, X.-L. (2019). "Nondestructive testing on ancient wooden components based on Shapley value," *Advances in Materials Science and Engineering* 2019, Article ID 8039734. DOI: 10.1155/2019/8039734

GB/T 1928 (2009). "General requirements for physical and mechanical tests of wood," Standardization Administration of China, Beijing, China.

GB/T 1938 (2009). "Method of testing in tensile strength parallel to grain of wood," Standardization Administration of China, Beijing, China.

GB/T 1936.1 (2009). "Method of testing in bending strength of wood," Standardization Administration of China, Beijing, China.

GB/T 1935 (2009). "Method of testing in compressive strength parallel to grain of wood," Standardization Administration of China, Beijing, China.

Guo, Z.-H., Shi, X.-D. (2003). *Reinforced Concrete Theory and Analyse*, Tsinghua University Press, Beijing, China.

He, J.-X., and Wang, J. (2018). "Theoretical model and finite element analysis for restoring moment at column foot during rocking," *Journal of Wood Science* 64(2), 97-111. DOI: 10.1007/s10086-017-1677-5

He, J.-X., Wang, J., and Yang, Q.-S. (2017a). "Theoretical and experimental analysis on mechanical behavior of column in traditional timber structure during rocking," *Engineering Mechanics* 34(11), 50-58. DOI: 10.6052/j.issn.1000-4750.2016.07.0527

He, J.-X., Wang, J., and Yang, Q.-S. (2017b). "Mechanical property of column footing joint in traditional wooden structure by quasi-static test," *Journal of Building Structures* 38(8), 141-149. (In Chinese) DOI: 10.14006/j.jzjgxb.2017.08.015

He, J.-X., Wang, J., and Yang, Q.-S. (2018). "Experimental study on lateral resistance capacity of column in traditional timber structures considering effects of height-diameter ratio," *China Civil Engineering Journal* 51(3), 27-35.

ISO 16670 (2003). "Timber structures — Joints made with mechanical fasteners — Quasi-static reversed-cyclic test method," International Organization for Standardization, Geneva, Switzerland.

JGJ/T 101 (2015). "Specification for seismic test of building," China Architecture & Building Press, Beijing, China.

Kusunoki, T., Kurihara, T., Mochizuki, E., Kushibe, A., Inoue, Y., Kyuke, H. (2003). "Full-scale shaking table tests of traditional wooden frame," *Journal of Structural and Construction Engineering* 18(38), 153-158. (In Japanese) DOI: 10.3130/aijt.18.153

Lee, D., Araki, Y., Endo, T., Yoshida, N., and Uetani, K. (2009). "Modeling of column base for traditional timber buildings based on local compression experiments at contact surface between column base and foundation stone," *Journal of Structural Construction Engineering* 74(639), 865-872. (In Japanese) DOI: 10.3130/aijs.74.865

Li, X., Dai, J., Qian, W., and Chang, L.-H. (2015). "Prediction of internal defect area in wooden components by stress wave velocity analysis," *BioResources* 10(3), 4167-4177. DOI: 10.15376/biores.10.3.4167-4177

Ma, B.-J. (2003). *Wood Works Technology of Ancient Chinese Architecture (Second Edition)*, Science Press, Beijing, China.

Maeno, M., Saito, S., and Suzuki, Y. (2007). "Evaluation of equilibrium of force acting on column and restoring force due to column rocking by full-scale tests of traditional wooden frames," *Journal of Structural and Construction Engineering (Transactions of AIJ)* 72(615), 153-160. DOI: 10.3130/aijs.72.153_1

Mukaibo, K., Kawakami, T., and Suzuki, Y. (2008). "Experimental and analytical study on seismic behavior of traditional wooden frames considering horizontal diaphragm deformation and column slippage," in: *The 14th World Conference on Earthquake Engineering*, Beijing, China.

Porcu, M. C. (2017). "Ductile behavior of timber structures under strong dynamic loads," *Wood in Civil Engineering* 2017, 173-196. DOI: 10.5772/65894

Qu, Z., Fu, X., Kishiki, S., and Cui, Y. (2020). "Behavior of masonry infilled Chuandou timber frames subjected to in-plane cyclic loading," *Engineering Structures* 211, Article ID 110449. DOI: 10.1016/j.engstruct.2020.110449

Shao, W.-S., Hsu, M.-F., and Komatsu, K. (2006). "Rotational performance of traditional Nuki joints with gap I: Theory and verification," *Journal of Wood Science* 52(1), 58-62. DOI: 10.1007/s10086-005-0734-7

Suzuki, Y., and Maeno, M. (2006). "Structural mechanism of traditional wooden frames by dynamic and static tests," *Structural Control and Health Monitoring* 13(1), 508-522. DOI: 10.1002/stc.153

Ssu-Ch'eng, L. (2006). *Graphic Illustration of the "Engineering Practice Rules" of the Ministry of Industry in Qing Dynasty*, Tsinghua University Press, Beijing, China.

The Institute for History of Natural Sciences (1985). *History of Ancient Chinese Architectural Technology*, Chinese Academy of Sciences Press, Beijing, China.

Wan, J., Yang, Q.-S., Wei, J.-W., and Li, T.-Y. (2020). "Initial motion analysis of traditional Chinese rocking timber frame subjected to horizontal ground motion: Theoretical and numerical investigations," *Engineering Structures* 203, Article ID 109898. DOI: 10.1016/j.engstruct.2019.109898

Wang, J., He, J.-X., Yang, Q.-S., and Yang, N. (2018). "Study on mechanical behaviors of column foot joint in traditional timber structure," *Structural Engineering and Mechanics* 66(1), 1-14. DOI: 10.12989/sem.2018.66.1.001

Yunli (1734). *"Engineering Practice" of Ministry of Industry in Qing Dynasty*, Ministry of Industry of the Qing Dynasty, Beijing, China.

Article submitted: April 28, 2020; Peer review completed: June 13, 2020; Revised version received: June 26, 2020; Accepted: July 5, 2020; Published: July 9, 2020.
DOI: 10.15376/biores.15.3.6648-6667